RSC Advances

ROYAL SOCIETY OF CHEMISTRY

www.rsc.org/advances

Journal Name

RSCPublishing

ARTICLE

Orange Red Emitting Naphthalene Diimide Derivative Containing Dendritic Wedges: Aggregation Induced Emission (AIE) and Detection of Picric acid (PA)

Cite this: DOI: 10.1039/x0xx00000x

P. Lasitha [a] and Edamana Prasad [*a]

Received 00th January 2012,
Accepted 00th January 2012

DOI: 10.1039/x0xx00000x

www.rsc.org/

Herein we report the synthesis, characterization and photophysical properties of novel naphthalene diimide (NDI) derivatives containing naphthalene units which are covalently attached to either end of the NDI. The self-assembly of such 'Donor-Acceptor-Donor' dendritic wedges shows aggregation induced emission (AIE), which in turn results in bright orange red emission from the NDI system, in aqueous medium and solid state. The structure of self-assembly has been analyzed using X-ray diffraction, variable temperature IR and NMR spectroscopy, scanning and transmission electron microscopy, steady state and time resolved emission spectroscopy. The results suggest that the emission quantum yields in the solid state vary inversely proportional to the number of donor units (naphthalene) attached to the NDI core. The NDI derivatives have been utilized to prepare organic nanoparticles (ONPs) in suitable solvent mixtures. Further, the ONPs as well as the solid thin film formed from the NDI derivative were utilized for the detection of picric aid through fluorescence quenching experiments, with a detection limit of 0.90 ppm.

Introduction

There are many rylene based compounds known to date, out of which naphthalene diimides (NDI), in particular, demonstrate interesting photophysical properties.[1] It has been shown that the photophysical and electronic properties of NDI are largely tuned by substitution with suitable donor or acceptor molecules.[2] The design of a variety of donor–acceptor (D–A) systems based on NDI derivatives enabled researchers to develop effective strategies for synthesizing materials of interesting properties and applications.[3] For example, the unique electronic and optical properties of conjugated D-A pairs of NDI have been utilized in organic field-effect transistors (OFETs)[4] and organic light-emitting diodes (OLEDs).[5]

While NDI based D-A systems are promising candidates for many optoelectronic applications,[6] luminescence from such compounds are usually quenched in the solid state presumably due to the aggregation effect {commonly referred to as aggregation induced quenching (AIQ)}. Conversely, a handful of reports describe enhanced emission due to aggregation of NDI based D-A molecules. For example, Gujrati *et al.* has reported bright orange red luminescence from non-covalently bound binary charge transfer complexes between NDI and pyrene in solid state.[7] Li *et al.* reported NDI molecules modified at shoulder position with electron donors such as thiophene and ferrocene with intense yellow emission (ϕ_f = 0.30) and optical waveguide properties in the aggregated state.[8] Recently, a core substituted NDI with imidazole donor has been reported by Li *et al.* showing bright red luminescence in solid state.[9] In such rare cases, aggregation can result in enhanced emission mainly due to aggregation induced emission (AIE) effect, where intramolecular motions of the fluorophore are restricted.[10,11]

Herein, we describe the design, synthesis and photophysical properties of three novel NDI derivatives which show AIE effect in solid state and solvent mixtures. The NDI derivatives contain naphthalene units which are covalently attached to either end of the NDI.[12] The design of the NDI based D-A system was carried out by increasing the donor units from compound **I** to **III** by providing a dendritic branching from the core.

Our objective is to identify the structure-property relations in NDI derivatives which control the interplay between self-assembly and aggregation induced emission properties of the system. In the present study, we compare the luminescence from self-assembled NDI derivatives in solution and solid state.

Solvent induced aggregation of the NDI derivatives leads to the formation of fluorescent organic nanoparticles (FONPs),[13-17] which have been further used for detecting picric acid (PA).[18] The NDI derivatives in the solid sate also exhibit the detection ability for PA. Even though there are many methods known for detection of PA[19,20] easy and portable detection methods have been rarely reported.

The aggregation and luminance properties of the NDI systems are analysed by UV-Vis and photoluminescence (PL) spectroscopy measurement. TGA and XRD were carried out to understand the thermal stability and molecular arrangement in the solid state. Variable Temperature based FT-IR and NMR measurement was performed to identify the mechanism of self-assembly. Detection of PA was studied through PL spectroscopy.

Experimental section

Materials

1,4,5,8-Naphthalenetetracarboxylic dianhydride was purchased from Sigma Aldrich and was used directly for synthesis. Nitroaromatics such as picric acid (PA), o-nitrotoluene (ONT), para nitro phenol(PNP) , and nitrobenzene (NB), and other organic compounds such as toluene (TOL) and phenol (PHE) were of analytical grade and obtained from Sriram chemicals, India. 2,4-dinitrotoluene (DNT) was obtained from Sigma Aldrich and used for the synthesis of 2,4,6-Trinitrotoluene (TNT) according to the synthesis procedure reported elsewhere.[21]

General Experimental methods

All the fluorescence spectral measurements were carried out on Horiba Jobin Yvon FluoroMax®-4 - Spectrofluorometer and UV spectra were recorded on JASCO-spectrophotometer using a quartz cuvette of path length 1 cm. NMR spectra were recorded on Bruker FT-NMR 500 MHz spectrophotometer in $CDCl_3$ and DMSO-d6 as solvents. Mass spectra were recorded using a Micromass Q-TOF mass spectrometer and a Voyager-DE PRO MALDI/TOF mass spectrometer with 2,5,-dihydroxy benzoic acid as the matrix. The fluorescence lifetime measurements were carried out by the time correlated single-photon counting technique (TCSPC) with a microchannel plate photomultiplier tube (MCPPMT) as the detector and a nanosecond laser as the excitation source (model 5000 U, IBH, UK).The scanning electron microscopic studies were carried out using a FEI-Quanta Microscope. TEM analysis were done in JEOL 3010 with a UHR pole piece operates at an accelerating voltage 300Kv. Thermogravimetric analysis (TGA) was performed on a PERKIN ELMER TGA7 apparatus with the scanning rate of 10 °C min^{-1},Powder-XRD patterns were recorded on a Bruker D8 Advance X-ray diffractometer using Cu-Ka radiation (λ=1.54 Å). Dynamic light scattering (DLS) experiments were done on a Malvern Zetasizer nano-series at 25^0C, with a path length of 1 cm (632.8 laser, scattering angle 90 degree) .

Results and discussion

The structure of the compounds used in the present study is given in Chart 1. Three derivative of NDIs were synthesized (compounds **1**, **II** and **III**), by end group modification of 1,4,5,8-naphthalne tetra carboxylic dianhydride. We designed compounds with increasing number of naphthalene units as shown in Chart 1. All the compounds were purified prior to the studies and characterized by NMR and ESI-MS and MALD-TOF analysis.

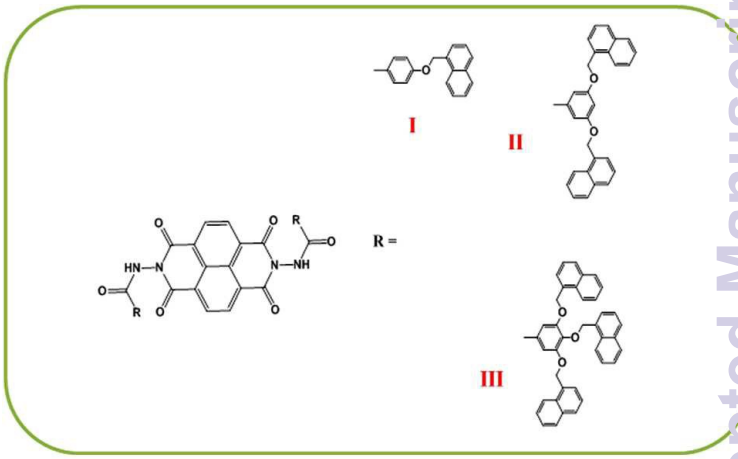

Chart 1.Structure of compounds **I-III** used in the present study.

Photo-physical studies in solution

In order to understand the nature of interaction among the molecules and to get more insight into the photoluminescence behaviour, effect of concentration on absorption and emission properties of compounds **I-III** has been studied. The UV-Vis and emission spectra of compound **I** at different concentrations are given in Fig. 1.

The major absorption peaks of compound **I** (Fig.1a) are assigned to π-π* transitions between 0-2, 0-1 and 0-0 vibrational energy levels of naphthalene diimide. As the concentration of compound **I** increases from 10^{-6} M to 10^{-4} M, a decrease in the π-π*absorption of NDI has been observed, along with a concomitant increase of a new peak at 487 nm. While compounds **II** and **III** follow similar behavior, the new absorption peak for compound **II** was not prominent compared to that of compounds **I** and **III** (Fig.S1†). The highest absorption intensity for the concentration dependent new peak was observed for compound III. The spectral behaviour in the solution state indicates that inter-molecular interaction increases as concentration increases and the aggregation propensity increased in the following order: compound **II** < compound **I** <compound **III**.

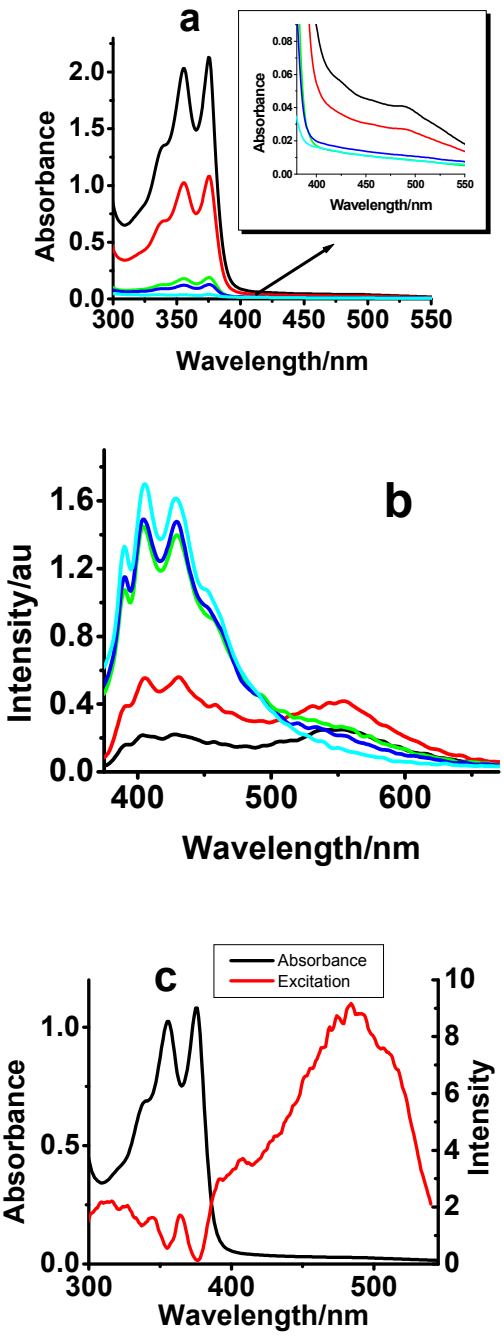

Fig. 1 (a) UV-Vis and (b) emission spectra of compound **I** in THF at different concentrations; black-10^{-4} M, red-0.5 x10^{-4} M, green- 10^{-5} M, sky blue -0.5x 10^{-5} M and navy blue-10^{-6} M,(Inset of a shows enlarged UV spectra from 400 nm-550 nm); (c) Normalised absorption and excitation spectra of compound **I** (0.5 x10^{-4} M) .

The emission spectra corresponding to compounds **I - III** were recorded at different concentrations. As the concentration was increased from 10^{-6}M to 10^{-4}M, a new emission band started appearing at higher wavelength region with maxima at 552 nm (Fig.1b). The emission features of compounds **I, II** and **III** were in agreement with their absorption properties (Fig.S1†.). For example, the emission intensity from the compounds decreases in the following order: compound **III** > compound **I** > compound **II**.

The absorption spectrum of compound **I** (0.5x10^{-4} M) is compared with the excitation spectrum collected at 590 nm (Fig.1c). It can be clearly seen from the spectra that the red shifted emission band for the NDI derivatives is originated by exciting the absorption peak which is assigned to aggregate formation. This suggests that the system can luminesce from its aggregated state.

Next, the UV-Vis and emission spectra of compounds **I -III** were recorded in DMSO, DMF, THF, DCM and$CHCl_3$. Absorption spectra of compound **I** exhibits an absorption tail mainly in DCM (Fig. 2a). As observed earlier, compound **II** exhibits negligible tail absorption, while compound **III** was absorbing with better extinction coefficient than compound **I** (Fig.S2†).

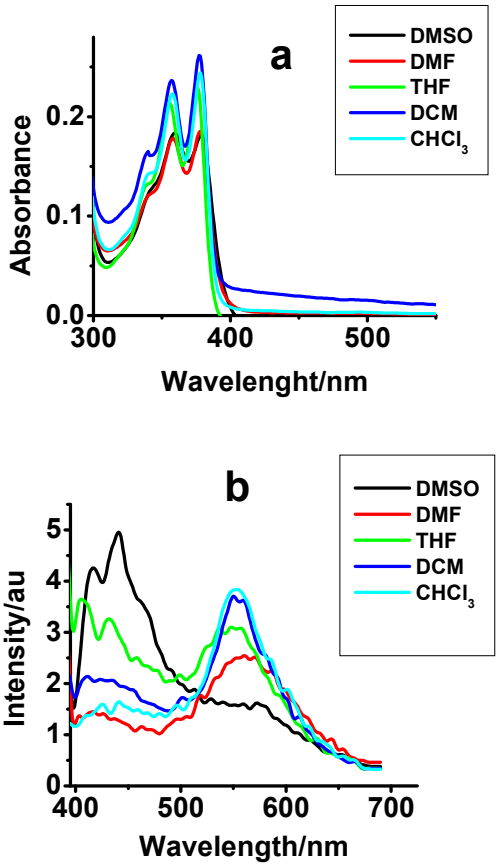

Fig. 2 (a) absorption and (b) emission spectra of compound **I** [2x10^{-5}M] in different solvents; λ_{ex} =350nm

Upon excitation at 350 nm (monomer excitation), emission spectra of compound **I** shows a new peak in all solvents with maxima at 550 nm. Emission quantum yield (ϕ_f) values were determined (quinine sulphate in 0.05N H_2SO_4 as standard) for compounds **I -III** in different solvents and the values are given,

along with absorption and emission maxima, in Table S1†. The highest quantum yield was observed for compound **III** in DMSO, with a maximum value of 8.9 x 10^{-3} (± 5%). As the values of emission quantum yields suggest, the emission intensity from the NDI derivatives was poor in solution phase.

The solvent dependent study, however, indicates that aggregation propensity of compounds **I-III** can be tuned by altering the polarity of the solvent milieu. It is, hence, hypothesized that addition of water to the system might lead to aggregation of the compounds due to the increased hydrophobic force of attraction by the aromatic rings in aqueous environment and this could lead to the formation of fluorescent organic nanoparticles (FONPs).

Synthesis of FONPs

We have generated fluorescent organic nanoparticles (FONPs) of compounds **I-III** by the addition of a poor solvent (water) to a dilute solution (10^{-5} M) of the compounds in THF. Absorption spectra show enhanced absorption as water content is increased from 10% to 50%. Conversely, the absorption decreased when water content was >50%. Presence of water also results in the formation of a tail absorption as seen in Fig. 3 and Fig.S3a,c†. The leveling-off the tail absorption is attributed to the Mie scattering with increased amount of water fraction in the system. The initial increase in absorbance is presumably due to the fact the presence of water might induce aggregation which leads to preferable molecular orientation for light absorption. However, at higher concentration of water, the system further aggregates, which leads to variation in HOMO-LUMO energy levels and shift in the absorption spectra. Upon addition of 70% water, all vibronic features of the spectra were completely lost and the absorption spectra were shifted to higher wavelength. The bathochromic shift observed for all the three compounds are attributed to the formation of J-aggregates.[11]

Consistent with the absorption studies, as the water concentration increases, the emission intensity from the monomer species increases initially and decreases above 50 % of water (Fig. 3b). At higher fraction of water, the emission from the aggregates results in a new emission band at 600 nm. The maximum intensity of the new emission band was obtained when the water content was 90%. Almost similar observations were found in the case of compound **II** (Fig.S3b†). However, the emission spectra of compound **III** show quenching (both monomer and aggregated state) as percentage of water increases in the system (Fig.S3d†). The compounds follow the following trend in their emission intensity from FONPs: compound **III** < compound **I** ~ compound **II.** The quenched emission from compound **III** could be attributed to the enhanced photoinduced electron transfer rate between naphthalene and NDI since the donor and acceptor molecules might be close to each other in compound **III**.[22]

Lifetime studies

The fluorescence measurement of FONP shows an initial enhancement in monomer emission, followed by quenching in presence of higher fraction of water. Fluorescence lifetime measurement was performed for compounds **I - III** to understand the nature of the aggregation. A 340 nm LED was used as excitation source and emission was collected at 430 nm. The lifetime decay profile for compounds **I-II** for different fraction of water is given in Fig.S4†. The lifetime decays were double exponential in nature, even in the absence of water. The lifetime decays remain constant till the water content is around 50%. Upon addition of >50 % water, the lifetimes values were decreased. This is consistent with the observations from the emission spectra. The quenching mechanism can be due various reasons such as collisional quenching, enhanced photoinduced electron transfer, formation of aggregates or energy migration among aggregates.[23,24] The lifetime data for the compounds **I -II** for the addition of different amount of THF/ water mixture is summarized in Table.S2†.

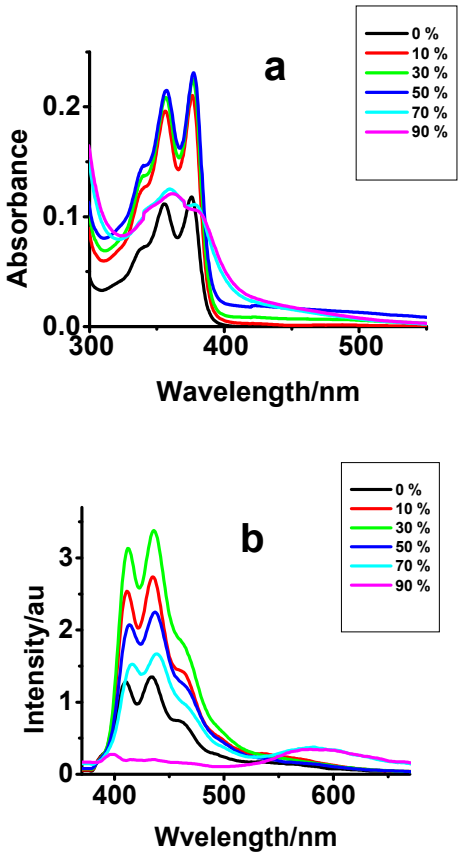

Fig.3 (a) UV-Vis and (b) emission spectra of compound **I** [10^{-5} M] in THF in presence of different amount of water.

Photo-physical studies in Solid State

We have observed that upon aggregation, NDIs shows red shifted emission band ~ 600 nm, which encouraged us to study the photo physical properties of NDI derivatives in solid state. A thin film of the compounds was made by drop casting a 10^{-3} M solution of the compounds on quartz plate. The absorption spectra of compound **I** in THF (10^{-3} M) and solid film are given in Fig.S5†. The absorption shoulder band was missing in the solid state spectrum. Instead, a tail extending to higher wavelength was found. Unlike in solution phase, all the compounds exhibit similar absorption behaviour in the solid thin film. The enhanced red shifted absorption, as observed in presence of water, confirms the formation of J-aggregates of the NDI in the solid state.

Interestingly, the compounds exhibit a unique emission pattern in the solid state. As shown in Fig.4, the intensity maxima (l_{max} = 600 nm) was highest for compound **I**, and then for compound **II** followed by a very feeble emission from compound **III.** Since emission maxima was shifted to 600 nm, the emission from compound **I** was intense orange red. The corresponding photographs of the compounds **I-III** under UV and visible light is given in Fig.4.

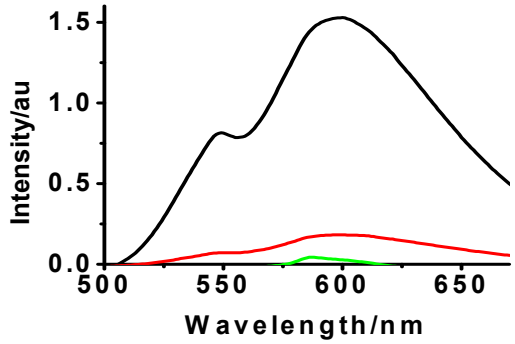

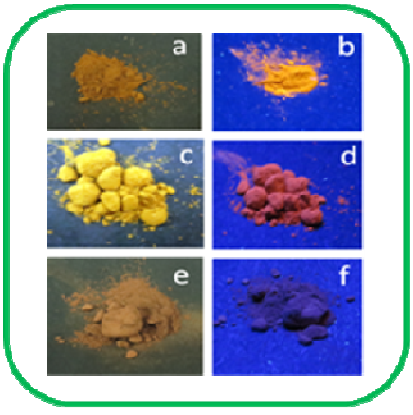

Fig. 4 (Above) Emission spectra of compound **I** (black), **II** (red) and **III**(green) in solid film.(Below) photograph of compounds **I**, **II** and **III** under a, c, e) visible light; b, d, f) UV light. λ_{ex}=365 nm

The emission intensity corresponding to compound **I** was ~40 fold higher than compound **III**. Solid state emission quantum yield is measured using integrating sphere method and the values are summarized in Table 1. The quantum yield of compound **I** was 0.01.

The excitation spectra of compounds **I-III** were recorded between 310-550 nm and the emission was collected at 590 nm (Fig. S6†). The excitation spectra for compounds **I-III** suggest aggregate formation in all the three compounds and the observed orange red emission is from the aggregates of NDIs. Lifetime for compound **I** and **II** is monitored in thin film by exciting at 340 nm and collecting emission at 600 nm (Fig.5).The decay for compound **I** was bi-exponential in nature with a short component (τ_1 =2.38 ns) and long component (τ_2=12.7 ns). Compound **II** also exhibits similar pattern (τ_1 = 1.78 ns, τ_2=6.31 ns). The initial component is typically from aggregates ,whereas the second component would be from pre-associated excimer (static in nature)[25] or exciplex. Lifetime values and relative amplitude are summarized in Table 1.

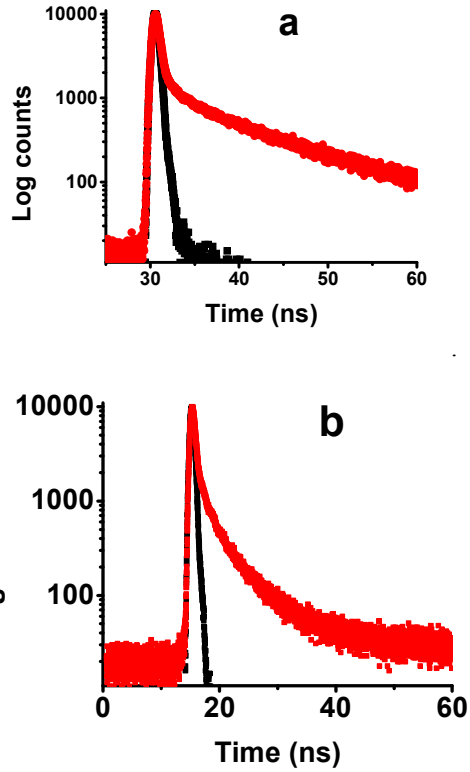

Fig.5 Lifetime plot for solid film of compound **I** (**a**) and compound II (**b**)λ_{ex} ,340 nm , emission collected at 600 nm.

Table 1 Quantum yield and lifetime data of compounds **I-III** in solid film.

Comp	Quantum yield ($\phi_{P.L.}$,%)[a]	Lifetime ns	CIHQ
I	1.10	2.4,12.7	1.14
II	0.30	1.8, 6.3	1.11
III	0.10		

a The emission quantum yield were measure by integrating sphere method (λ_{ex} =340 nm)

Thermal stability and molecular arrangement-TGA ,PXRD measurements

Thermal stability of compounds **I-III** was analysed using TGA. The TGA thermogram for compounds **I-III** is shown in Fig. S7†. For compound **I**, about 10% weight loss was observed at 220 ^{o}C and 7.27% weight loss was observed at 270 ^{0}C in the case of compound **II**. Among the compounds, compound **III** shows highest thermal stability which gives first decomposition at 500 ^{0}C with 52.53% weight loss. This large difference in thermal stability among three compounds suggests that, compound **III** is more rigid in nature due to the sterically encumbered dendron units.The nature of the molecular arrangement in solid state has been analysed by SXRD and WXRD pattern for **I-III** (Fig.6, Fig. S8†.). The diffraction pattern of compound **I** consist of sharp five reflection peaks in small angle range with 2θ values 6.99 ^{0}, 9.14 ^{0},11.59 ^{0},14.098 ^{0}and 14.87 ^{0}, which correspond to d-spacing values of 12.63, 9.7, 7.68, 6.27 and 5.95 Å respectively. The ratio of the d values are 1:1/2 $^{1/2}$:1/3 $^{1/2}$:1/4$^{1/2}$, which indicate tetragonal columnar arrangement. The peak corresponds to 6.99^{0} represents the inter layer spacing with d value 12.63Å. Using chemBio3D Ultra 11.0, the fully extended length of compound **I** has been calculated as 32.5Å. Such a large difference in the theoretical and experimental values suggests that, there must be intercalation between naphthalene units within the π-π stacked NDI core. The molecules presumably will arrange in a slip-off fashion, resulting in the formation of J-type aggregates. The reflection peak of compound **I** was observed at 23.8 ^{0}, which represents the π-π stacking distance of 3.7Å.[23a] Compound **II** and **III** shows respective d-spacing of 20.24 Å (4.36 ^{0}) and 14.71 Å (6 ^{0}). The π-π stacking distance are 3.84 Å and 3.77 Å respectively.The d-spacing and π-π stacking distance indicates that NDI core units are in typically co-facial arrangement with peripheral naphthalene. The sharp reflections peaks observed for compound **I** compared **II** and **III** indicating increased crystallinity because of less steric hindrance in former case. A cartoon representation of the expected molecular arrangement is shown in Scheme 1. Further self-assembly of such an arrangement can form tetragonal columnar type geometry for the NDI derivative, as shown in Scheme 1.

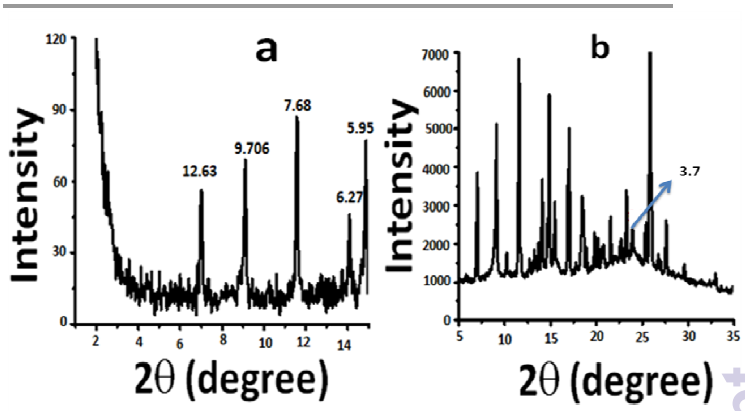

Fig.6 SXRD (a) and WXRD (b) of compound **I.**

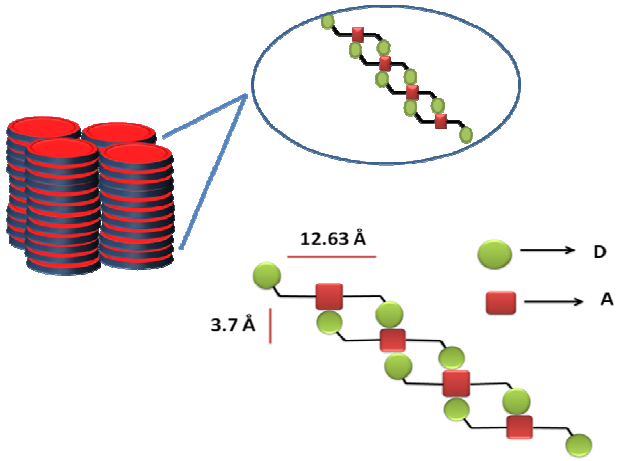

Scheme.1 Schematic representation of the initial molecular arrangement in compound **I**

Variable temperature IR and NMR measurements

Since, it is already known that the hydrogen bonding motifs largely decides the self-assembly of molecules[26],we performed variable temperature(VT) FTIR and NMR studies to understand the nature (inter Vs intra) of hydrogen bonding. We assume that the amide groups present in the molecule would typically decide the molecular arrangement in compounds **I-III.** VT-FTIR measurements were carried out between 30-100 ^{o}C, and Fig. S9† shows the expanded IR spectra of compounds **I-III**.

At 30 ^{0}C, the compounds show single NH stretching (3200 cm^{-1}) and multiple C=O stretching (1730 cm^{-1}, 1690 cm^{-1} and 1680 cm^{-1}) peaks. As temperature is increased to 100^{0} C, the NH band shows decrease in intensity and a slight shift to higher wave number. For example, compound **II** exhibits a NH band shift from 3198 to 3241 cm^{-1} as the temperature varies from 30^{0} C to 100 ^{0}C. Similar type of shift was observed for compound **III** (ie., from 3213 to 3264 cm^{-1}). The presence of inter-molecular hydrogen bonding is emphasized by the decrease in intensity of NH stretching band along with increase

in temperature. Such intensity decrease with temperature and shift to the higher wave number is common with intermolecular hydrogen bonding.[27]

The VT-NMR of compound **II** in DMSO-d6 from 30^{0}C -120^{0}C is shown in Fig .7. The NH peak (δ=11.45 ppm) for compound **II** appeared as doublet at lower temperatute. As the temperature is increased, NH peak became singlet and shifted upfield to11.1 ppm. Similarly, in compound **III,** a peak shift from 11.6ppm to 11.30 ppm has been obrved (Fig.S10†). As the temperature is increased, intensity of NH peak correspond to NDI core (at ≈ δ 8.8 ppm) also increases.

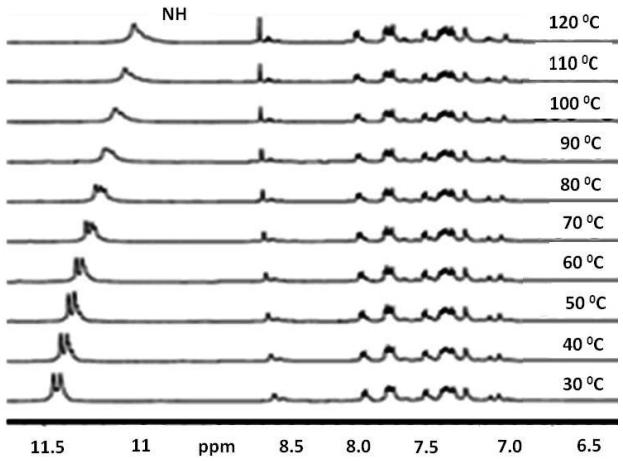

Fig. 7 variable temperature NMR spectra of compound **II** in DMSO-d6 from 30^{o}C to 120^{o}C. (concentration =3.5 x10^{-2}M)

The existence of higher degree of molecular aggregation and intermolecular hydrogen bonding is clearly evident from spectral shift of NH proton to lower ppm with increase in temperature.[26] Since, the exact co-facial arrangement is prevented, the NH protons may experiance different environment at lower temperatures resulting in spliting, which is overcome at higher temperatures.The intermolecular hydrogen bonding decreases due to the disassembly of moleculaes which results in upfield shift with increase in temperature. We have recorded the VT-NMR for compound **II** (Fig.S10†) in $CDCl_3$.The NMR spectra in $CDCl_3$ was broad and unresolved. With variation in temperature from -40 ^{0}C to 50 ^{0}C peaks remain poorly resolved. These observations are in accordance with the finding from UV-Vis and PL measurements were the prominent aggregation is observed in non polar solvent such as $CHCl_3$

SEM, TEM and DLS analysis

In order to understand the morphology of the compounds **I -III** in the aggregated state, SEM, TEM and DLS analysis were carried out. SEM images of the compound **II** with different fraction of water is shown in Fig.8. Up on increasing the fraction of water to 30% to 50%, the spherical nano aggregates begins to form with particles size range of 130 nm to 260 nm (Fig.S11†). Interestingly, smaller spherical particles were formed as water percentage increases to 70% to 90%. The spherical particles were vesicular in geometry, as evident from the color contrast in the SEM images.

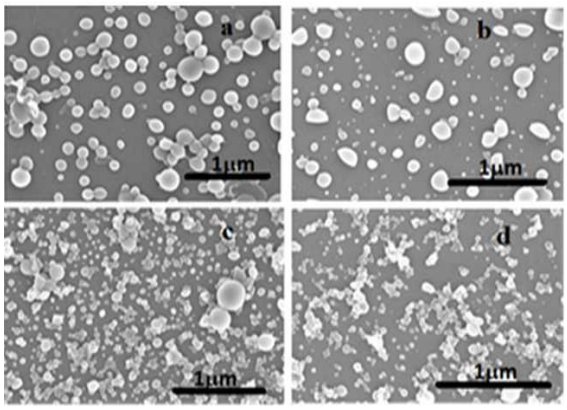

Fig.8 SEM images of compound **II** in 30 % water (a), 50 % water (b), 70 % water (c) and 90 % water (d).

The TEM images of compounds **I-III** in presence of 90% water clearly shows the formation of nano aggregates (Fig.S12†). More uniform spherical aggregates were observed in the case of compound **II**. We assume that the NDI core and naphthalene units are arranged in such a fashion that amide groups are exposed to the water in extreme interior and exterior of vesicle. The average particle size obtained for compounds **I -III** from DLS measurements are 290 nm, 530 nm and 400 nm, respectively (Fig.S12†). DLS study indicates that aggregation propensity in compound **II** is higher compared **I** and **III.** The difference in average size measured from SEM and DLS is likely to be due to the presence of the hydration sphere in the solution phase.

Picric acid detection

Fluorescence from nanofibers can be annihilated in presence of analytes such as nitroaromatic explosives. Moreover, sensing of analytes by fluorescence quenching has considered to have more advantageous compared to other methods because of excellent sensitivity during sensing. We have observed that compound **II** shows excellent aggregation behaviour on addition of water. Sensing of nitroaromatic in aqueous medium has real life application, since nitroaromatics are water pollutants. Hence we sought to analyse the effect of nitroaromatics on fluorescence of NDI nanoaggregates in aqueous medium. Interestingly, we found that fluorescence quenching is highly selective for picric acid (PA).Upon addition of different equivalent of PA to the solution of compound **II** in THF/Water (1:9), emission from the aggregated nanoparticles decreases (Fig .8). With the addition of 30 equivalent of PA emission intensity quenched by 99 %. The Stern- Volmer plot for the addition of PA was plotted, and K_{sv} (Stern-Volmer constant) was calculated using the initial linear part of the plot (below 0.8 μM). The value for K_{sv} was 9.6 x10^4 M^{-1} for the case of compound **II**. Selectivity of PA has been confirmed by quenching study with other nitro aromatic. The percentage of quenching and selectivity is shown in

Fig.S13a†. The detection limit was calculated by performing fluorescence titration with addition of aliquots of PA and taking the inflection point where the sudden emission drop is observed (Fig.S13b†).[18c.] The detection limit was found to be 0.90 ppm.

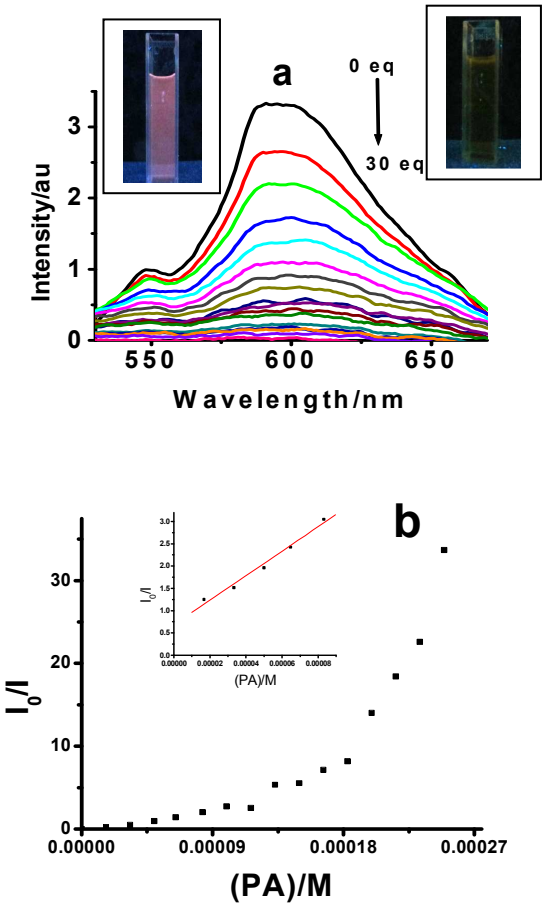

Fig.9 (a) emission response and (b) Stern -Volmer plot of compound **II** ($9x10^{-6}$ M) in THF/Water (1:9) with addition of different equivalent of PA (0-30eq)., λ_{ex} : 350 nm.

The quenching of emission from the aggregated nano system could be attributed to the interaction of hydroxyl group of the PA with amine moiety of NDI.[18] The ground state complex formation between PA and NDI derivative leads to the breakdown of the nano-aggregates in the system, resulting in the emission quenching. The other nitro aromatics like TNT, ONT, DNT and NB were not able to quench the emission from the organic nanoparticles presumably due to the absence of a hydroxyl group. This indicates that hydroxyl group plays a crucial role in the present case. We believe that the hydroxyl group present in the PA tamper the hydrogen bonding network in the nano aggregates, leading to the luminescence quenching. The luminescence quenching experiment was also performed using TLC stripes where compound II (200 µl, 10-3 M) was drop casted in presence and absence of the analyte. The emission intensity was quenched to ~50% in the presence of the analyte (PA) (60 µl, 10 -3 M).

The static nature of complex formation between NDI and PA was further confirmed by the lifetime measurement in solid film (Fig.S14†). Lifetime values of compound **II** was unaffected by the PA addition, which corroborates that the quenching is not dynamic in nature. We have recorded SEM images compound **II** (Fig.S14a,b†) before and after addition of PA. SEM images clearly indicate that the nano aggregates breaks into smaller aggregates upon addition of PA. These observations clearly corroborate the ground sate interaction and complex formation of PA with nano aggregates. The deviation in the Stern-Volmer plot at higher concentration of PA could be due to the collisional quenching, along with static quenching, resulting in a bi-model quenching mechanism.

Conclusions

A novel NDI based solid state emitter has been designed and synthesized. The effect of the number of donor units on controlling the self-assembly and photophysical properties has been investigated. The results suggest that increase in the donor number in a dendritic fashion could lead to self-assembly at the expense of emission intensity. The results also indicate that increase of donor units (naphthalene) beyond two on either side of the core results in emission quenching in solution state and increase of the donor units beyond one on either side of the core results in significant emission quenching in solid state. The emission quantum yield was highest when only one naphthalene donor was introduced to the NDI unit, on either side. Solvent induced self-assembly yielded fluorescent organic nanoparticles (FONPs), which has been utilized as a effective sensor for picric acid with a detection limit of 0.90 ppm under aqueous medium.

Acknowledgements

We thank Prof. T. Pradeep, IIT Madras for TEM and Dr. M.L.P. Reddy ,NIIST, TVM for integrating sphere facilities. P.L thanks University Grants Commission (UGC), New Delhi, India, for a fellowship.

a Department of Chemistry ,IIT-Madras,Cennai-600036,India.
E-mail: pre@iitm.ac.in.

† Electronic supplementary information (ESI) available: Details of synthetic procedure, UV-Vis, PL, CV, spectroscopic characterization or other electronic format See DOI: 10.1039/b000000x/

References

1. J. G. laquindanum, H. E. Katz, A. Dodabalapur, A. J. Lovinger, *J. Am. Chem. Soc*., 1996, **118**, 11331; H. E. Katz, A. J. Lovinger, J. Johnson, C. Kloc, T. Siegrist, W. Li, Y.Y. Lin, A. Dodabalapur, *Nature,* 2000, **404**, 478.

2. Y. A. Getmanenko, S. Singh, B. Sandhu, C. Y. Wang, T. Timofeeva , B. Kippelen and S. R. Marder, *J. Mater. Chem. C.,* 2014, **2**, 124; L. Yang, C. Xiao, W. Jiang and Z. Wang, Tetrahedron, 2014, **70**, 6265.

3. G. Koshkakaryan, L. M. Klivansky, D. Cao, M. Snauko, S. J. Teat, J. O. Struppe and Y. Liu, *J. Am. Chem. Soc.,* 2009, **131**, 2078; P. M. Alvey, R. J. Ono, C. W. Bielawski, and B. L. Iverson. *Macromolecules*, 2013, **46**, 718.

4. G. Ren, E. Ahmedb and S. A. Jenekhe, *J. Mater. Chem.,*2012, **22**, 24373.
5. N. Sakai, J. Mareda E. Vauthey and S. Matile, *Chem. Commun.,* 2010, **46**, 4225.
6. J . G. Laquindanum, H. E. Katz, A. Dodabalapur and A. J. Lovinger, *J. Am. Chem. Soc.,* 1996, **118**, 11331.
7. M. D. Gujrati, N. S. S. Kumar, A. S. Brown, B. Captain and J. N. Wilson, *Langmuir,* 2011, **27**, 6554.
8. Y. Li, G. Zhang, G. Yang, Y. Guo, C.-A. Di, X. Chen, Z, Liu, H. Liu, Z. Xu, W. Xu, H. Fu, and D. Zhang, *J. Org. Chem.,* 2013, **78**, 2926.
9. N. Li, L. Zong, Q. Li, Z. Li, *Sensors and Actuators B*, 2015, **207**,827.
10. Y. Hong, J. W. Y. Lam, B. Z. Tang, *Chem. Commun,* 2009, **29**, 4332; Y. Hong, J. W. Y. Lam, B. Z. Tang, *Chem. Soc. Rev.,* 2011, **40**, 5361; Z. Zhao, J. W. Y. Lam, B. Z. Tang, *J. Mater. Chem.,* 2012, **22**, 23726; J. Zhou, B. R. He, B. Chen, P. Lu, H. H. Y. Sung, I. D. Williams, A. J. Qin, H. Y. Qiu, Z. J. Zhao and B. Z. Tang, *Dyes Pigm.,* 2013, **99**, 520; Z. J. Zhao, Z. F. Chang, B. R. He, B. Chen, C. M. Deng, P. Lu, H. Y. Qiu and B. Z. Tang, *Chem. Eur. J.,* 2013, **19**, 11512.
11. A. Das, M.R. Molla, A. Banerjee, A. Paul, and S. Ghosh, *Chem. Eur. J.,* 2011, **17**, 6061; A. Das, M. R. Molla, B. Maity, D. Koley, and S. Ghosh, *Chem. Eur. J.,* 2012, **18**, 9849.

12. B. K. An, S. K. Kwon, S. D. Jung, and S.Y. Park, *J. Am. Chem. Soc.,* 2002, **124**, 14410.
13. H. H. Lin, Y.C. Chan, J. W. Chena and C. C. Chang, *J. Mater. Chem.,*2011, **21**, 3170.

14. S. S. Palayangoda, X. Cai, R.M. Adhikari, and D. C. Neckers, *Org. Lett.,* 2008, **10**,281.

15. F. Wang, J. Wen, L. Huang, J. Huanga and J. Ouyang, *Chem. Commun..,*2012, **48**, 7395.

16. X. Chen, X. Y. Shen, E. Guan, Y. Liu, A. Qin, J. Z. Sun and B .Z. Tang, *Chem. Commun.,* 2013, **49**, 1503.
17. Y. S. Zheng and Y. J. Hu, *J. Org. Chem.,* 2009, **74**, 5660.
18. S. Shanmugaraju, S. A. Joshi and P. S. Mukherjee, *J. Mater. Chem.,* 2011, **21**, 9130; S. Kaur, V. Bhalla, V. Vij and M. Kumar, *J. Mater. Chem. C.,* 2014, **2**, 3936; V. Bhalla, A. Gupta, and M. Kumar, *Org. Lett., 2012*, **14**, 3112.

19. V. Vij, V. Bhalla, and M.Kumar, *ACS Appl. Mater. Interfaces.,* 2013, **5**, 5373.

20. Y. Xu, B. Li, W. Li, J .Zhao, S. Sun and Y. Pang, *Chem. Commun.,* 2013, **49**, 4764.

21. R. C. Dorey and W. R. Carper, *J. Chem. Eng. Data..,* 1984, **29**, 93.

22. Y. Kim, J. Hong, J.H. Oh and C. Yang, *Chem. Mater., 2013,* **25**, 3251
23. X. Zhao, P. Xue, K. Wang, P. Chen, P. Zhanga and Ran, *New J. Chem.,* 2014, **38**, 1045.

24. N. Zhao, M. Li, Y. Yan, J. W. Y. Lam, Y. L. Zhang, Y.S. Zhao, K. S. Wong and B. Z. Tang, *J. Mater. Chem. C.,* 2013, **1**, 4640.
25. C. Kulkarni and S. J. George., *Chem. Eur. J.,* 2014, **20**, 4537; C. Kulkarni, R. Munirathinam, and S. J. George., *Chem. Eur. J.* 2013, **19**, 11270; B. Narayan , S. P. Senanayak, A. Jain, K. S. Narayan, and S.J. George, *Adv. Funct. Mater.,*2013, **23**, 3053.; M. Kumar and S. J. George, *Chem. Eur. J.,* 2011, **17**, 11102.
26. B. M. Schulze, N. T. Shewmon, J. Zhang, D. L. Watkins, J. P. Mudrick, W. Cao, R. B. Zerdan, A. J. Quartararo, I. Ghiviriga, J. Xue and R. K. Castellano, *J. Mater. Chem. A*., 2014, **2**, 1541.
27. N. B. Kolhe, R. N. Devi, S. P. Senanayak, B. Jancy, K. S. Narayan and S. K. Asha., *J. Mater. Chem.* 2012, **22**, 15235.
28. V. Bhalla, A. Gupta, M. Kumar, D. S. S. Rao, and S. K. Prasad, *ACS Appl. Mater. Interfaces.,*2013, **5**, 672.